Boundary-Layer Meteorol (2015) 157:1–21
DOI 10.1007/s10546-015-0048-2

ARTICLE

Turbulent Energy Spectra and Cospectra of Momentum and Heat Fluxes in the Stable Atmospheric Surface Layer

Dan Li[1] · **Gabriel G. Katul**[2] · **Elie Bou-Zeid**[3]

Received: 2 December 2014 / Accepted: 26 May 2015 / Published online: 12 June 2015

Abstract The turbulent energy spectra and cospectra of momentum and sensible heat fluxes are examined theoretically and experimentally with increasing flux Richardson number (Rf) in the stable atmospheric surface layer. A cospectral budget model, previously used to explain the bulk relation between the turbulent Prandtl number (Pr_t) and the gradient Richardson number (Ri) as well as the relation between Rf and Ri, is employed to interpret field measurements over a lake and a glacier. The shapes of the vertical velocity and temperature spectra, needed for closing the cospectral budget model, are first examined with increasing Rf. In addition, the wavenumber-dependent relaxation time scales for momentum and heat fluxes are inferred from the cospectral budgets and investigated. Using experimental data and proposed extensions to the cospectral budget model, the existence of a '-1' power-law scaling in the temperature spectra but its absence from the vertical velocity spectra is shown to reduce the magnitude of the maximum flux Richardson number (Rf_m), which is commonly inferred from the Rf–Ri relation when Ri becomes very large (idealized with $Ri \to \infty$). Moreover, dissimilarity in relaxation time scales between momentum and heat fluxes, also affected by the existence of the '-1' power-law scaling in the temperature spectra, leads to $Pr_t \neq 1$ under near-neutral conditions. It is further shown that the production rate of turbulent kinetic energy decreases more rapidly than that of turbulent potential energy as $Rf \to Rf_m$, which explains the observed disappearance of the inertial subrange in the vertical velocity spectra at a smaller Rf as compared to its counterpart in the temperature spectra. These results further demonstrate novel linkages between the scale-wise turbulent kinetic energy and potential energy distributions and macroscopic relations such as stability correction functions to the mean flow and the Pr_t–Ri relation.

✉ Dan Li
danl@princeton.edu

1 Program of Atmospheric and Oceanic Sciences, Princeton University, Princeton, NJ 08544, USA

2 Nicholas School of the Environment & Department of Civil and Environmental Engineering, Duke University, Durham, NC 27708, USA

3 Department of Civil and Environmental Engineering, Princeton University, Princeton, NJ 08544, USA

Keywords Cospectra · Energy spectra · Flux Richardson number · Gradient Richardson number · Kolmogorov's theory · Stable atmospheric surface layer · Turbulent Prandtl number

1 Introduction

While the significance of stably-stratified turbulent flows is rarely disputed, operational formulations describing their bulk properties continue to be debated (Fernando 1991; Sorbjan 2006, 2010; Huang et al. 2013; Sandu et al. 2013; Mahrt 2014). Dimensional considerations or similarity arguments that predict bulk properties of stably stratified turbulent flows are extensively employed in a myriad of problems but their theoretical underpinnings remain elusive despite advances in numerical simulations and experiments (Derbyshire 1999; Mahrt 1999; Poulos et al. 2002; Sorbjan 2006, 2010; Fernando and Weil 2010; Chung and Matheou 2012; Holtslag 2013). A case in point is the stability correction functions for momentum and heat that account for buoyancy distortions to the logarithmic mean velocity and temperature profiles in the stably-stratified atmospheric surface-layer (ASL) flows. Deriving these stability correction functions theoretically continues to be the subject of active research (Sukoriansky et al. 2005a, b; Katul et al. 2011; Li et al. 2012b; Sukoriansky and Galperin 2013). In addition, the variation of their ratio, or the turbulent Prandtl number (Pr_t), with increasing stability, quantified using the gradient Richardson number (Ri) or the flux Richardson number (Rf), remains a long-standing problem as well (Yamada 1975; Kays 1994; Venayagamoorthy and Stretch 2009). Since the Kansas experiment (Kaimal et al. 1972), it was often assumed that $Pr_t \approx 1$ in the stable ASL (Foken 2006) provided Ri is below some critical value coinciding with a presumed laminarization of turbulent flows (Howard 1961; Miles 1961; Miles and Howard 1964). However, a large corpus of data and simulations now suggest that Pr_t increases with increasing Ri (Zilitinkevich et al. 2007, 2008, 2013) and connections between laminarization and such a critical Ri are questionable at best (Monin and Yaglom 1971), as reviewed elsewhere (Galperin et al. 2007).

Some studies have investigated these issues using phenomenological theories (Katul et al. 2011; Li et al. 2012b; Salesky et al. 2013) that offer a promising theoretical tactic to begin explaining the shapes of stability correction functions for momentum and heat, as well as their ratio Pr_t. These phenomenological theories proved to be rather successful for unstable conditions but required ad hoc modifications for stable conditions. Despite their drawbacks, these phenomenological theories do offer a new perspective on links between vertical velocity and temperature spectra and the mean velocity and temperature profiles in the ASL. Given that the vertical velocity and temperature spectral shapes appear to be general in the ASL, it has been conjectured that the near-universal character of the stability correction functions as well as the Pr_t–Ri and Rf–Ri relations may be connected to the general shapes of the vertical velocity and temperature spectra (Katul et al. 2011; Li et al. 2012b).

Two recent studies further explored linkages between spectra and bulk properties of the flow by closing cospectral budgets for momentum and sensible heat fluxes using idealized vertical velocity and temperature spectral shapes (Katul et al. 2013, 2014). Guided by direct numerical simulation (DNS) results (Katul et al. 2014), the spectra of vertical velocity and temperature were assumed to follow the '$-5/3$' power-law scaling (Kolmogorov 1941a, b) within the inertial subrange (ISR), but to 'level-off' to a constant when the wavenumber is smaller than a certain threshold. In these DNS results, the presence of a solid boundary appears to randomize the energy distribution among scales larger than the distance from the boundary resulting in near-flat vertical velocity and temperature spectra. The cospectral budget analysis

in these studies alleviated some of the shortcomings of a previous phenomenological theory developed for a non-stratified smooth pipe flow (Gioia et al. 2010), as discussed elsewhere (Katul and Manes 2014). It also produced satisfactory results under both unstable (Katul et al. 2013) and stable (Katul et al. 2014) conditions thereby underlining possible linkages between the scale-wise turbulent kinetic energy (TKE) and turbulent potential energy (TPE) distributions (defined by the spectra) and macroscopic relations such as the stability correction functions (Li et al. 2015). A parallel theoretical effort relying on the quasi-normal scale elimination theory (Sukoriansky et al. 2005a, b, 2006; Galperin and Sukoriansky 2010; Sukoriansky and Galperin 2013) was also successful in relating macroscopic properties of stable flows to turbulence theory, but did not consider all the features of wall-bounded flows similar to those in the ASL.

In addition to the idealized spectral shapes for vertical velocity and temperature, a wavenumber-dependent relaxation time scale first derived from Kolmogorov's scaling argument by Corrsin (1961) was also employed in Katul et al. (2014). This relaxation time scale continues to enjoy wide-spread usage in turbulence studies (Bos et al. 2004; Bos and Bertoglio 2007). The main assumption employed to close the cospectral budgets requires that this wavenumber-dependent relaxation time scale is identical for momentum and heat.

These assumptions, while offering a number of mathematical conveniences, do not necessarily reflect actual spectra in the ASL known to be affected by low-frequency modulations (Pond et al. 1966; Kader and Yaglom 1991; Katul et al. 1995, 1998; Riley and Lindborg 2008; Calaf et al. 2013; Grachev et al. 2013). The objective here is to investigate the impact of such low frequency modulations on vertical velocity and temperature spectra and their propagation to momentum and heat flux cospectra using observations from two field experiments that cover a wide range of stable conditions over uniform and flat surfaces, and then to propose a revised cospectral budget model in light of the observations. The data suggest the existence of a '-1' power-law scaling in temperature spectra and some dissimilarity in relaxation time scales between momentum and heat. How these two findings affect Pr_t under neutral conditions and the maximum flux Richardson number (Rf_m) is addressed by generalizing the cospectral budget model in Katul et al. (2014). Moreover, changes in the TKE and TPE spectra with increasing stability are also examined using the generalized cospectral budget model.

2 Theory

The stability correction functions for momentum $\phi_\mathrm{m}(\zeta)$ and heat $\phi_\mathrm{h}(\zeta)$ in the ASL are defined as (Stull 1988)

$$\phi_\mathrm{m}(\zeta) = \frac{\kappa_\mathrm{v} z}{u_*}\frac{\partial \overline{U}(z)}{\partial z} = \frac{\kappa_\mathrm{v} z}{u_*} S, \tag{1}$$

$$\phi_\mathrm{h}(\zeta) = \frac{\kappa_\mathrm{v} z}{\theta_*}\frac{\partial \overline{\theta}(z)}{\partial z} = \frac{\kappa_\mathrm{v} z}{\theta_*} \Gamma, \tag{2}$$

where the overline denotes Reynolds averaging and primes denote turbulent fluctuations from the averaged state, u_* is the friction velocity, $S = \partial \overline{U}(z)/\partial z$ is the mean velocity gradient, $\Gamma = \partial \overline{\theta}(z)/\partial z$ is the mean potential temperature gradient, $\kappa_\mathrm{v} = 0.4$ is the von Kármán constant, $\zeta = z/L$ is the stability parameter, z is the height above the ground (or above the zero-plane displacement), $L = -u_*^3/(\kappa_\mathrm{v}\beta\overline{w'\theta_\mathrm{v}'})$ is the Obukhov length (Obukhov 1946; Monin and Obukhov 1954; Businger and Yaglom 1971), $\beta = g/\overline{\theta_\mathrm{v}}$ is the buoyancy parameter, g is the acceleration due to gravity, θ_v is the virtual potential temperature, and

$\theta_* = -\overline{w'\theta'}/u_*$ is a temperature scaling parameter. For simplicity, the virtual temperature is approximated by the air temperature due to the minor impact of the water vapour flux on the buoyancy flux in the stable ASL. The potential temperature is also approximated by the air temperature since the data used in our study were collected near the surface ($z < 4$ m).

These definitions for $\phi_{\mathrm{m}}(\zeta)$ and $\phi_{\mathrm{h}}(\zeta)$ imply that the turbulent viscosity for momentum and the turbulent diffusivity for heat are $K_{\mathrm{m}} = \kappa_{\mathrm{v}} u_* z/\phi_{\mathrm{m}}(\zeta)$ and $K_{\mathrm{h}} = \kappa_{\mathrm{v}} u_* z/\phi_{\mathrm{h}}(\zeta)$, respectively. As such, the turbulent Prandtl number Pr_{t} is given as

$$Pr_{\mathrm{t}} = \frac{K_{\mathrm{m}}}{K_{\mathrm{h}}} = \frac{\phi_{\mathrm{h}}(\zeta)}{\phi_{\mathrm{m}}(\zeta)}. \tag{3}$$

Under stable conditions, Pr_{t} is commonly expressed as the ratio of gradient (Ri) to flux (Rf) Richardson numbers (Kays 1994),

$$Pr_{\mathrm{t}} = \frac{Ri}{Rf}, \tag{4}$$

where

$$Ri = \frac{\beta \Gamma}{S^2} = \frac{N^2}{S^2}, \tag{5}$$

$$Rf = -\frac{\beta \overline{w'\theta'}}{-S\overline{u'w'}} = \frac{\beta}{S} \frac{\int_0^\infty F_{wT}(k)\,\mathrm{d}k}{\int_0^\infty F_{uw}(k)\,\mathrm{d}k}, \tag{6}$$

and where $N = (\beta\Gamma)^{1/2}$ is the Brunt–Väisälä frequency. Note that $P_m = -S\overline{u'w'}$ is the shear or mechanical production rate of TKE and $\beta\overline{w'\theta'}$ is the conversion rate of TKE to TPE by buoyancy in stable conditions where $\overline{w'\theta'} < 0$. $F_{uw}(k)$ and $F_{wT}(k)$ are the momentum-flux and heat-flux cospectra at wavenumber k, respectively. In principle, $F_{uw}(k)$ and $F_{wT}(k)$ should be integrated over the surface of a sphere of radius k, where k is the scalar wavenumber. However, because cospectra and spectra reported in ASL field studies are usually calculated from single-point time series measurements (Kaimal et al. 1972; Wyngaard and Cote 1972; Kaimal 1973) and frequencies are converted to streamwise one-dimensional wavenumbers using Taylor's frozen turbulence hypothesis (Taylor 1938; Kaimal and Finnigan 1994), one-dimensional cospectra and spectra are used here and k should be interpreted as the wavenumber in the streamwise direction.

Deriving a relation between Rf and Ri or a relation between Pr_{t} and Ri by closing the cospectral budgets of momentum and heat fluxes was the main result of Katul et al. (2014). Here, the final results of this derivation are repeated without discussing its details. For a stationary, locally equilibrated, and sufficiently developed turbulent stable ASL flow, the momentum and heat flux cospectra are expressed as

$$F_{uw}(k) = \frac{(1 - C_{IU})}{A_U \tau_{uw}^{-1}(k)} S F_{ww}(k), \tag{7}$$

$$F_{wT}(k) = \frac{(1 - C_{IT})}{A_T \tau_{wT}^{-1}(k)} \left[\Gamma F_{ww}(k) - \frac{\beta F_{TT}(k)}{1 - C_{IT}} \right], \tag{8}$$

where $F_{ww}(k)$ and $F_{TT}(k)$ are the spectra of vertical velocity and temperature, respectively, $\tau_{uw}(k)$ and $\tau_{wT}(k)$ are two wavenumber-dependent relaxation time scales defined later (Eq. 11), $A_U \approx A_T$ ($\approx$1.8) are the Rotta constants (Launder et al. 1975; Pope 2000), and $C_{IU} \approx C_{IT}$ ($\approx$0.6) are constants associated with isotropization of production terms whose value

can be determined by the rapid distortion theory in homogeneous turbulence (Launder et al. 1975; Pope 2000).

At this stage of the derivation, these two spectra can take on any shape. When idealized spectral shapes are assumed (Katul et al. 2014) with a constant value for $k < k_a$ and the ISR '$-5/3$' scaling (Kolmogorov 1941a, b) for $k > k_a$,

$$F_{ww}(k) = \min\left(C_{ww}k^{-5/3}, C_{ww}{k_a}^{-5/3}\right), \tag{9}$$

$$F_{TT}(k) = \min\left(C_{TT}k^{-5/3}, C_{TT}{k_a}^{-5/3}\right), \tag{10}$$

where k_a is a threshold wavenumber associated with the start of the ISR, $C_{ww} = C_o\epsilon^{2/3}$, $C_{TT} = C_T\epsilon^{-1/3}N_T$, ϵ and N_T are the TKE dissipation rate and the temperature variance dissipation rate, respectively. The constants C_o and C_T are the Kolmogorov and Kolmogorov–Obukvov–Corrsin constants for vertical velocity and temperature spectra, respectively. For a one-dimensional wavenumber interpretation their values are $C_o = 0.65$ and $C_T = 0.8$ (Ishihara et al. 2002; Chung and Matheou 2012). The k_a threshold is commonly set to be $1/z$ for ASL flows under near-neutral conditions since eddies of size z or larger interact with the surface and are usually anisotropic (Townsend 1976; Kaimal and Finnigan 1994).

$\tau_{uw}(k)$ and $\tau_{wT}(k)$ are two wavenumber-dependent relaxation time scales used in the Rotta closure model (Launder et al. 1975; Pope 2000), which are assumed to be identical and given by (Bos et al. 2004; Bos and Bertoglio 2007)

$$\tau(k) = \min\left(\epsilon^{-1/3}k^{-2/3}, \epsilon^{-1/3}{k_a}^{-2/3}\right). \tag{11}$$

The '$-2/3$' scaling of relaxation time scales results in a '$-7/3$' scaling in the momentum and heat flux cospectra, which are consistent with many dimensional considerations, experiments and simulations (Lumley 1967; Kaimal and Finnigan 1994; Pope 2000). Some studies argued that the flux-transfer terms in the cospectral budgets of momentum and heat fluxes could be significant within the ISR (Bos et al. 2004; Bos and Bertoglio 2007; Cava and Katul 2012), which led to a scaling other than '$-7/3$' for the momentum- and heat-flux cospectra. Since the majority of field studies support a '$-7/3$' cospectral scaling in the stable ASL (Kaimal and Finnigan 1994), deviations of cospectral scaling from the '$-7/3$' value within the ISR due to contributions from flux-transfer terms are ignored for now. Also note this choice of $\tau(k)$ is similar but not identical to relaxation time scales employed in *TKE–*ϵ and other higher-order turbulent closure models (Launder et al. 1975; Pope 2000; Katul et al. 2004; Zilitinkevich et al. 2008), which define τ as the ratio of available TKE to ϵ.

Substituting $F_{ww}(k)$, $F_{TT}(k)$, and $\tau(k)$ into Eqs. 7 and 8 yields $F_{uw}(k)$ and $F_{wT}(k)$, which can be further substituted into Eq. 6 to obtain the relation between *Rf* and *Ri* or the relation between Pr_{t} and *Ri* (Katul et al. 2014), as follows

$$R_f = \frac{1 + \omega Ri - \sqrt{-4Ri + (-1 - \omega Ri)^2}}{2}, \tag{12}$$

$$Pr_{\mathrm{t}} = \frac{2Ri}{1 + \omega Ri - \sqrt{-4Ri + (-1 - \omega Ri)^2}}, \tag{13}$$

where $\omega = (1 - C_{IT})^{-1}(C_T/C_o) + 1 \approx 4$. As shown in Katul et al. (2014), *Rf* increases with increasing *Ri* and then begins to flatten at $Ri \approx 0.25$. The 'flattening' indicates that the *Rf* cannot increase infinitely as *Ri*, which can be viewed as an external parameter that characterizes the mean flow (Zilitinkevich et al. 2007). Instead, *Rf* is determined by the turbulence state and is limited by a 'maximum flux Richardson number' ($Rf_{\mathrm{m}} = 1/\omega \approx 0.25$) even when *Ri* becomes very large (idealized with $Ri \to \infty$). It is also shown that the turbulent

Table 1 The range of Rf, the averaged Rf, and the number of 30-min segments in each of the eight stability regimes

Regime a reflects near-neutral conditions while regime h reflects very stable conditions. Regimes a to e only include the lake data and regimes f to h only include the glacier data. Details about the two datasets can be found in the Appendix

Regime	Rf	Averaged Rf	Segments
a	$0.00 < Rf < 0.01$	0.006	16
b	$0.01 < Rf < 0.02$	0.015	25
c	$0.02 < Rf < 0.04$	0.029	19
d	$0.04 < Rf < 0.08$	0.047	15
e	$0.08 < Rf < 0.25$	0.110	13
f	$0.08 < Rf < 0.25$	0.193	6
g	$0.25 < Rf < 0.50$	0.405	6
h	$0.50 < Rf < 1.00$	0.620	9

Prandtl number Pr_t increases with increasing Ri (Katul et al. 2014). The Rf–Ri and Pr_t–Ri relations predicted by the cospectral budget model (Eqs. 12, 13) reasonably agree with many laboratory and field experiments and numerical simulations when the vertical velocity and temperature spectra do not appreciably deviate from their idealized shapes (Katul et al. 2014). It is precisely the observed deviations in the spectra of vertical velocity and temperature from their idealized shapes that frame the scope here.

3 Results

The closure to the cospectral budget model in Katul et al. (2014) relied on two assumptions: first, $F_{ww}(k)$ and $F_{TT}(k)$ follow the ISR '$-5/3$' scaling when $k > k_a$ and 'level off' when $k < k_a$ (see Eqs. 9, 10). The values of k_a may be different for momentum and heat, and the consequences of having different k_a for momentum and heat have been discussed in Katul et al. (2014). Second, the relaxation time scales for momentum and heat fluxes are identical and follow the '$-2/3$' scaling law in the ISR (see Eq. 11). In this section, these two assumptions are examined using data from two field experiments (over a lake and a glacier) as described in the Appendix. The datasets are separated into eight groups with increasing Rf, which range from near-neutral to very stable regimes (see Table 1).

3.1 The Turbulent Energy Spectra $F_{ww}(k)$ and $F_{TT}(k)$

To investigate the first assumption, the measured $F_{ww}(k)$ and $F_{TT}(k)$ are shown in Figs. 1 and 2, respectively. Their scaling laws in two ranges of wavenumber ($k < k_a$ and $k > k_a$) are also noted. In this section, $k_a = 1/z$ is used as a length scale for normalizing both spectra (Townsend 1976; Kaimal and Finnigan 1994). However, as seen later, a more general transition wavenumber can be used for $F_{ww}(k)$ and $F_{TT}(k)$ when revising the idealized spectral shapes.

$F_{ww}(k)$ appears to reasonably follow its idealized shape in regimes a to e (i.e., when Rf is well below $Rf_m \approx 0.25$). However, in regimes f to h (as Rf approaches or exceeds Rf_m), its ISR is appreciably reduced. This finding is consistent with recent experiments reporting that ISR scaling no longer holds when $Rf > Rf_m$ and vertical turbulent fluxes become small and difficult to measure (Grachev et al. 2013). Some of the fine-scale turbulence that continues to survive when $Rf > Rf_m$ in $F_{ww}(k)$ does not follow the ISR scaling. Studies also have found that turbulence is no longer well-developed and becomes globally intermittent at these extreme stabilities (Mahrt 1999; Ansorge and Mellado 2014; Deusebio et al. 2014).

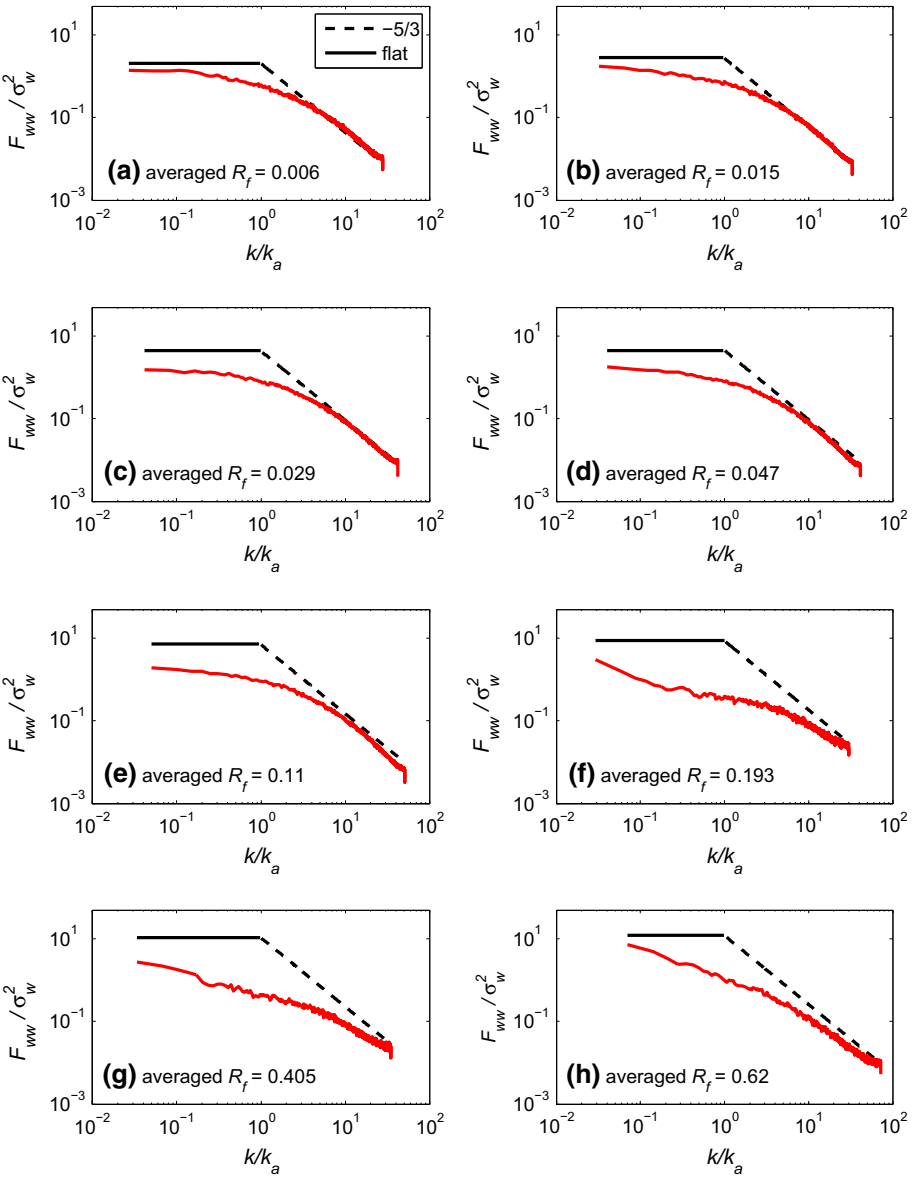

Fig. 1 The normalized spectra of vertical velocity ($F_{ww}(k)$) for the eight stability regimes. σ_w is the standard deviation of the vertical velocity. **a**–**h** correspond to the stability regimes a to h in Table 1, respectively. All spectra are averaged over all segments in the stability regime. $k_a = 1/z$

Compared to $F_{ww}(k)$, $F_{TT}(k)$ shows many interesting features. First, $F_{TT}(k)$ exhibits a distinct '-1' scaling when $k < k_a$, which was not previously considered in the cospectral budget model since $F_{TT}(k)$ was assumed to follow the same idealized spectral shape as $F_{ww}(k)$ (Katul et al. 2014). Second, as Rf approaches and increases beyond Rf_{m}, the '-1' scaling is gradually diminished at low wavenumbers. However, even when $Rf > Rf_{\mathrm{m}}$, the large wavenumber part of $F_{TT}(k)$ still maintains the '$-5/3$' scaling.

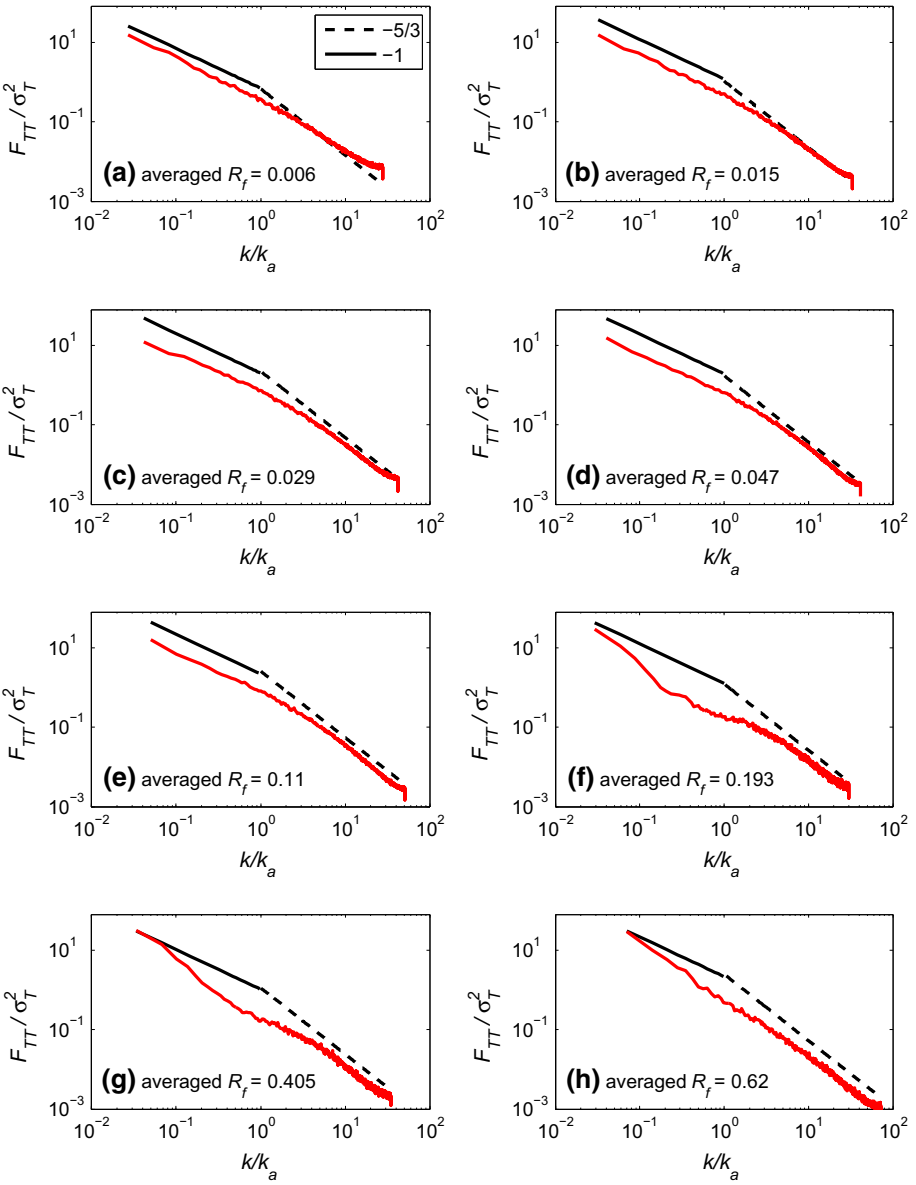

Fig. 2 The normalized spectra of temperature ($F_{TT}(k)$) for the eight stability regimes. σ_T is the standard deviation of the temperature. **a**–**h** correspond to the stability regimes *a* to *h* in Table 1, respectively. All spectra are averaged over all segments in the stability regime. $k_a = 1/z$

The dynamics at play when $Rf > Rf_\mathrm{m}$ may be related to the Ozmidov length scale, which can be viewed as the smallest scale influenced by the stabilizing buoyancy force. The Ozmidov length scale is defined as $L_0 = [\epsilon/N^3]^{1/2}$, where ϵ is the dissipation rate of TKE and N is the Brunt–Väisälä frequency defined earlier. For the idealized ASL considered in the cospectral budget model, it can be shown that $L_0/(\kappa_\mathrm{v} z) = \left[(\phi_\mathrm{m}(\zeta) - \zeta)^{1/2}(Pr_\mathrm{t}\zeta\phi_\mathrm{m}(\zeta))^{-3/4}\right]$. As a

result, the Ozmidov length scale approaches z when $\zeta \approx 0.3{-}0.4$, which corresponds to Rf of 0.13 to 0.14. As can be seen from Table 1, this occurs between regime e and regime f. Up to regime e, the influence of stability does not extend to the ISR of $F_{ww}(k)$ or $F_{TT}(k)$ because $L_0 > z$. At higher Rf, the influence of stability is manifest in $F_{ww}(k)$, which is the component directly modulated by buoyancy, but the influence of stability on $F_{TT}(k)$ is not direct and hence the ISR scaling for temperature survives until even higher stabilities are reached. Further explanation for this difference between $F_{ww}(k)$ and $F_{TT}(k)$ when $Rf > Rf_{\mathrm{m}}$ will be presented later. In addition, a more general transition wavenumber will be used later when generalizing the idealized spectral shapes for $F_{ww}(k)$ and $F_{TT}(k)$ to accommodate other length scales in addition to z in the stable ASL.

The '-1' power-law scaling observed in the spectra of temperature here has been reported in other ASL experiments for the spectra of the streamwise velocity component, pressure, and skin and air temperatures, especially for near-neutral conditions (Kader and Yaglom 1991; Katul et al. 1995, 1996, 1998, 2012; Katul and Chu 1998). It was also documented in many laboratory studies for the spectra of the streamwise velocity component (Perry and Abell 1975, 1977; Perry et al. 1986) but not $F_{ww}(k)$. It is noted that the '-1' scaling examined here is not connected to the '-1' scaling in the 'viscous-convective' subrange at large molecular Schmidt or Prandtl numbers reviewed elsewhere (Davidson et al. 2012).

Some studies have reported a transition from the '$-5/3$' scaling to '-3' scaling in $F_{TT}(k)$ (and also $F_{ww}(k)$) as the wavenumber decreases below the Ozmidov wavenumber $(1/L_0)$ using measurements in the free troposphere (i.e. above the atmospheric boundary layer) and the lower stratosphere (Cot 2001), and in the deep ocean (Bouruet-Aubertot et al. 2010). The '-3' scaling is associated with internal gravity waves that affect scales larger than L_0 (Riley and Lindborg 2008; Galperin and Sukoriansky 2010; Sukoriansky and Galperin 2013). The difference between our study and those aforementioned studies is the presence of the ground (i.e., the wall), which is necessary for the onset of a '-1' scaling (at least for near-neutral to mildly stable flows). The 'wall effect' is absent in the aforementioned studies that reported a transition from '$-5/3$' to '-3' scaling in the temperature spectra, thereby preventing their applicability here to the ASL. In addition, even when L_0 approaches or becomes smaller than z, as in regimes f to g, a '-3' scaling is not observed in $F_{TT}(k)$ or $F_{ww}(k)$ (see Figs. 1, 2). The absence of '-3' scaling in $F_{TT}(k)$ and $F_{ww}(k)$ at these high stabilities may be explained by the presence of external perturbations such as radiative perturbations occurring during passage of clouds, which prevent gravity waves from persisting over time scales on the order of 30 min (the averaging interval used in our study). Cava et al. (2004) reported the percentages of gravity-wave occurrence over an even-aged pine forest for 21 nights, which were only 6 % on average, and were zero for 10 of 21 nights. The data quality control applied here may have also removed non-stationary runs, or runs affected by large flux-transport terms, since the differences in measured fluxes among the four different heights were restricted to <10 %.

3.2 The Relaxation Time Scales $\tau_{uw}(k)$ and $\tau_{wT}(k)$

To examine the second assumption, the wavenumber-dependent relaxation time scales for momentum and heat fluxes are estimated as

$$\tau_{uw}(k) = \frac{F_{uw}(k)}{SF_{ww}(k)} \frac{A_U}{1 - C_{IU}}, \tag{14}$$

$$\tau_{wT}(k) = \frac{F_{wT}}{\left[\Gamma F_{ww}(k) - \frac{\beta F_{TT}(k)}{1 - C_{IT}}\right]} \frac{A_T}{1 - C_{IT}}. \tag{15}$$

The measured $F_{ww}(k)$ and $F_{TT}(k)$ are combined with measured $F_{uw}(k)$ and $F_{wT}(k)$ to infer the relaxation time scales from the two datasets. S and Γ are estimated by fitting second-order polynomial functions to the mean velocity and temperature at the four measurement levels, and then computing derivatives to fitted functions. The inferred relaxation time scales for momentum and heat fluxes pre-multiplied by $k^{2/3}$ are shown in Fig. 3.

It is clear that the relaxation time scales for momentum and heat fluxes, as computed from Eqs. 14 and 15 respectively, differ in magnitude and scaling laws with k. In particular, it appears that the largest difference resides in the low wavenumber part. When $Rf < Rf_{\mathrm{m}}$ (i.e., regimes a to e), τ_{uw} roughly follows the '$-2/3$' power-law scaling (which corresponds to $\tau_{uw}k^{2/3}$ being a constant, see the black lines in Fig. 3) over a decade of scales ($0.5 < k/k_a < 5$) and approaches a constant (which corresponds to $\tau_{uw}k^{2/3}$ following a '2/3' power-law scaling, see the black dashed line in Fig. 3b) at very low wavenumber ($k/k_a < 0.5$).

On the other hand, τ_{wT} trends may be consistent with '$-2/3$' power-law scaling at large wavenumbers ($k/k_a > 5$) though the noise level introduced by the gradients in Eq. 15 prohibits definitive assessments. It is noted that some studies have shown that the flux-transfer terms in the cospectral budgets can cause deviations of the scaling of $F_{wT}(k)$ from the '$-7/3$' power-law scaling in the ISR (Bos et al. 2004; Bos and Bertoglio 2007; Cava and Katul 2012; Li et al. 2015), which might also contribute to the indistinct '$-2/3$' scaling law in τ_{wT} here. In the low wavenumber part, the τ_{wT} appears to be constant (i.e., $\tau_{wT}k^{2/3}$ follows a '2/3' scaling) or slightly increasing as k increases, due to the presence of a '-1' power-law scaling in the temperature spectra within this range (see Eq. 15).

As stability increases further, large scatter exists in the inferred τ_{uw} and τ_{wT}, but it appears that the '$-2/3$' scaling holds for both τ_{uw} and τ_{wT} for very large k, at least within the confines of the noise introduced from the measured gradients (see Eqs. 14, 15). Overall, when $Rf < Rf_{\mathrm{m}}$, the '$-2/3$' power-law scaling exists for both τ_{uw} and τ_{wT} as predicted from ISR scaling, but the transitions from the '$-2/3$' power-law scaling to a constant or some other scaling law differ for τ_{uw} and τ_{wT}. The transition wavenumber for τ_{uw} is smaller than the transition wavenumber for τ_{wT}, and the consequences of this difference in transitional wavenumber are discussed below.

4 Discussions

The role of a '-1' power-law scaling in $F_{TT}(k)$ as well as dissimilarity in relaxation time scales for momentum and heat fluxes as suggested by the measurements are now discussed in the context of Pr_{t}–Ri and Rf–Ri relations. Changes in the TKE and TPE spectra as the ASL transitions to very stable conditions are also discussed.

4.1 The Impact of $F_{TT}(k) \sim k^{-1}$ and the Dissimilarity in Relaxation Time Scales

Based on experimental data, the idealized shapes of $F_{ww}(k)$, $F_{TT}(k)$, $\tau_{uw}(k)$, and $\tau_{wT}(k)$ used earlier (Katul et al. 2014) are revised and summarized in Fig. 4. In Katul et al. (2014), the spectral shape of $F_{ww}(k)$ was assumed to follow the '$-5/3$' ISR scaling when $k > k_a$ and a constant when $k < k_a$ at least when $Rf < Rf_{\mathrm{m}}$. As a result, $F_{ww}(k)$ at the transition wavenumber k_a is continuous but not smooth, though this has a minor impact on any bulk formulation requiring a wavenumber-integrated form of $F_{ww}(k)$. This idealized shape for $F_{ww}(k)$ is reasonably supported by the two datasets (see Fig. 1) and is not modified here except that a more general transition wavenumber between the ISR and large scales $k_{a,w}$ is used (see Fig. 4a), which can be different from its counterpart in the temperature spectra.

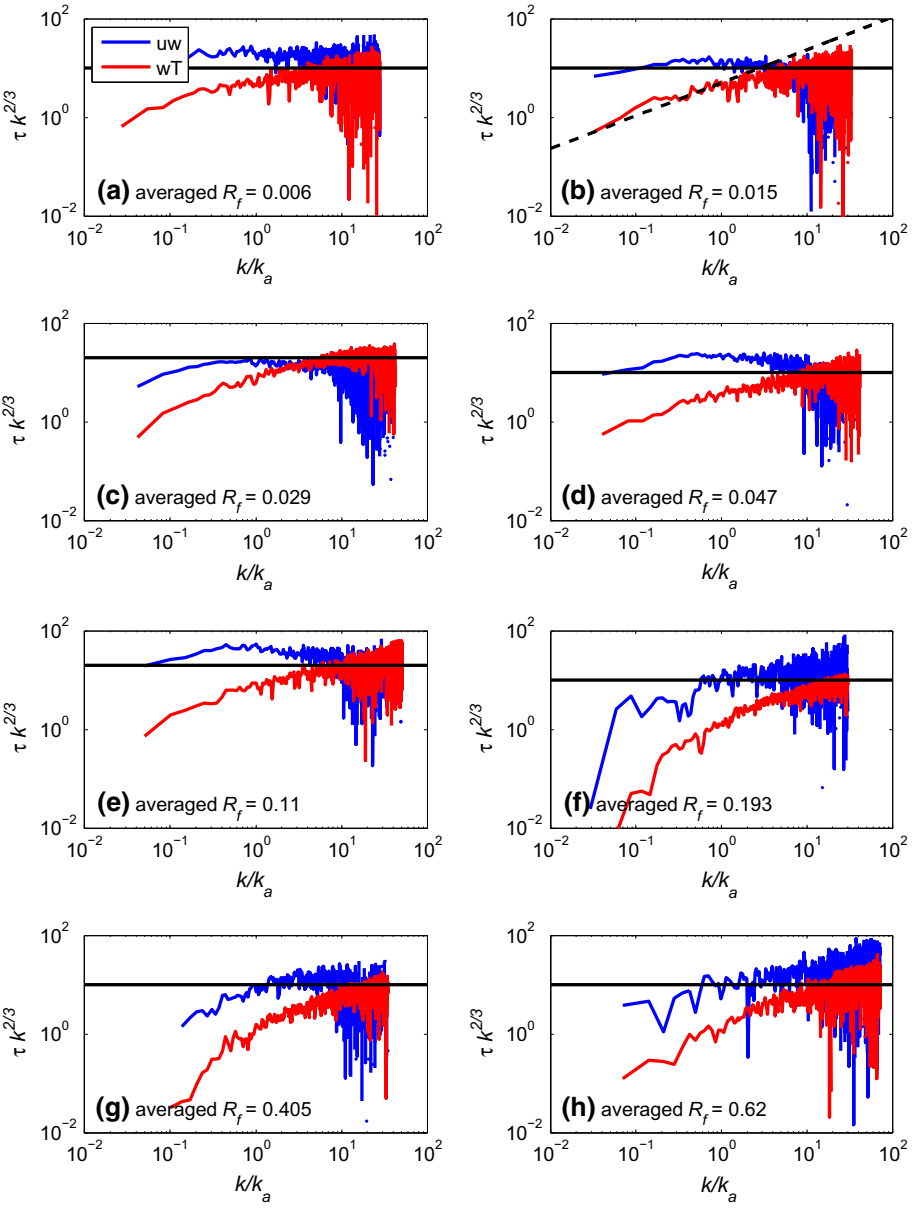

Fig. 3 The Rotta model's relaxation time scales for momentum flux (τ_{uw}) and heat flux (τ_{wT}) pre-multiplied by $k^{2/3}$ for the eight stability regimes. The *black lines* indicate the flat regimes and the *black dashed line* in **b** indicates the '2/3' scaling. **a**–**h** Correspond to stability regimes *a* to *h* in Table 1, respectively. $k_a = 1/z$

However, measured $F_{TT}(k)$ significantly differs from this idealized shape due to the presence of a '-1' power-law scaling in the low wavenumber range, as shown in Fig. 2. As a result, the effects of the '-1' scaling on the bulk properties of the stable ASL are now explicitly considered. To simplify the analysis, the '-1' power-law scaling in $F_{TT}(k)$ is

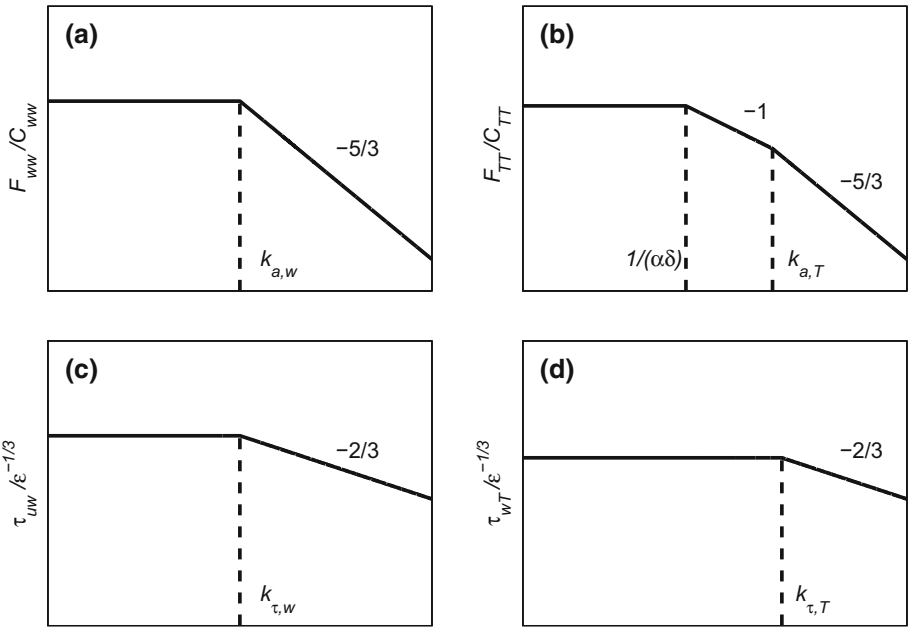

Fig. 4 The idealized shapes of F_{ww} (**a**), F_{TT} (**b**), τ_{uw} (**c**), τ_{wT} (**d**)

assumed to extend from $\alpha\delta$ to $k_{a,T}$ as shown in Fig. 4b, where α is a constant, and is flow- and stability-dependent; δ is the depth of the atmospheric boundary layer. The length scale $\alpha\delta$ is a characteristic size of large turbulent eddies in the stable ASL, which are assumed to be larger than z. A more general transition wavenumber between the ISR and large scales $k_{a,T}$ is used here to accommodate the impact of other length scales such as the Ozmidov length scale (in addition to z).

The relaxation time scales for both momentum and heat fluxes are still assumed to follow the '$-2/3$' power-law scaling at large k and become constant at small k for mathematical convenience. However, the transition wavenumber is different for momentum and heat fluxes (i.e., $k_{\tau,w} \neq k_{\tau,T}$), which can also be different from $k_{a,w}$ and $k_{a,T}$. Comparing Figs. 1, 2, and 3 also reveals that $k_{\tau,w} < k_{a,w}$ but $k_{\tau,T} > k_{a,T}$ and $k_{\tau,T} > k_{a,w}$. The relations between different transition wavenumber are significant because they define the idealized shapes of spectra and relaxation time scales.

With these idealized shapes for spectra and relaxation time scales shown in Fig. 4, integrating the cospectra models (Eqs. 7, 8) from $k = 0$ to $k = \infty$ yields the momentum and heat fluxes. It can be shown that,

$$\overline{u'w'} = \int_0^\infty F_{uw}(k)\,\mathrm{d}k = -\frac{1 - C_{IU}}{A_U} C_o \epsilon^{\frac{1}{3}} S f_1, \tag{16}$$

$$\overline{w'\theta'} = \int_0^\infty F_{wT}(k)\,\mathrm{d}k = -\frac{1 - C_{IT}}{A_T} C_o \epsilon^{\frac{1}{3}} \Gamma g_1 Q, \tag{17}$$

where

$$Q = \left(1 - \frac{1}{1 - C_{IT}} \frac{C_T}{C_o} \frac{g_2}{g_1} \frac{R_f}{(1 - R_f)}\right), \tag{18}$$

$$f_1 = \frac{1}{k_{a,w}^{4/3}} \left[\frac{15}{4} - 2\left(\frac{k_{\tau,w}}{k_{a,w}}\right)^{1/3}\right], \tag{19}$$

$$g_1 = \frac{1}{k_{\tau,T}^{4/3}} \left[\frac{5}{2}\left(\frac{k_{\tau,T}}{k_{a,w}}\right)^{2/3} - \frac{3}{4}\right], \tag{20}$$

and

$$g_2 = \frac{1}{k_{\tau,T}^{4/3}} \left[\left(\frac{5}{2} + \ln(k_{a,T}\alpha\delta)\right)\left(\frac{k_{\tau,T}}{k_{a,T}}\right)^{2/3} - \frac{3}{4}\right]. \tag{21}$$

Hence,

$$Pr_{\mathrm{t}}^{-1} = \frac{R_f}{R_g} = \frac{A_U(1 - C_{IT})}{A_T(1 - C_{IU})} \frac{g_1}{f_1} Q. \tag{22}$$

Note that with $\beta\overline{w'\theta'} = R_f S\overline{u'w'} = -R_f P_m$, the stationary TKE budget equation under local equilibrium yields $\epsilon = P_m + \beta\overline{w'\theta'} = P_m(1 - R_f)$. To ensure $\epsilon > 0$, it is necessary that $Rf < 1$ to maintain turbulent conditions. It is again pointed out that the cospectral budget model assumes fully-developed turbulent conditions so that a sufficiently large ISR exists. In addition, to ensure $Pr_{\mathrm{t}} > 0$, Rf must be smaller than a threshold given by

$$Rf_{\mathrm{m}} = \frac{1}{1 + \frac{1}{1 - C_{IT}} \frac{C_T}{C_o} \frac{g_2}{g_1}}. \tag{23}$$

It is interesting to compare these new results to those in Katul et al. (2014) in which $k_{a,w} = k_{\tau,w} = k_{a,T} = k_{\tau,T} = 1/(\alpha\delta)$ is assumed so that $f_1 = g_1 = g_2$. It is clear from Eq. 23 that Rf_{m} is modulated by the inequality between g_1 and g_2, which was not accounted for previously (Katul et al. 2014). This inequality between g_1 and g_2 stems from the inequality among $k_{a,w}$, $k_{a,T}$ and $k_{\tau,T}$, as well as the existence of the '-1' scaling in $F_{TT}(k)$ shown in Fig. 2, as can be seen from Eqs. 20 and 21. In particular, when $k_{a,w} = k_{a,T} = k_{\tau,T} > 1/(\alpha\delta)$, it can be demonstrated that

$$\frac{g_2}{g_1} = 1 + \frac{4}{7}\ln\left(k_{a,T}\alpha\delta\right) > 1, \tag{24}$$

provided that $k_{a,T}\alpha\delta > 1$. As such, the relation between the maximum Rf obtained here ($Rf_{\mathrm{m}}^{\mathrm{new}}$) and that from Katul et al. (2014) ($Rf_{\mathrm{m}}^{\mathrm{old}}$) is

$$Rf_{\mathrm{m}}^{\mathrm{new}} = \frac{1}{1 + \left(\frac{1}{1 - C_{IT}}\right)\frac{C_T}{C_o}\frac{g_2}{g_1}} < \frac{1}{1 + \left(\frac{1}{1 - C_{IT}}\right)\frac{C_T}{C_o}} = Rf_{\mathrm{m}}^{\mathrm{old}}. \tag{25}$$

That is, the existence of '-1' scaling in $F_{TT}(k)$ tends to reduce the numerical value of Rf_{m}. The magnitude of the reduction depends on g_2/g_1 and thus on $\alpha\delta$, which unfortunately is not available from the measurements here. Future investigations with direct measurements of the boundary-layer height or estimates from profile measurements (Zhang et al. 2014) are needed to further constrain the reduction in Rf_{m} arising from a '-1' scaling in $F_{TT}(k)$.

Another important parameter to compare is Pr_{t} as neutral conditions are approached (i.e., when $Rf = 0$). In the derivation here,

$$Pr_{t,\mathrm{neu}} = \frac{A_T(1 - C_{IU})}{A_U(1 - C_{IT})} \frac{f_1}{g_1}. \tag{26}$$

Therefore, the deviation of $Pr_{t,\mathrm{neu}}$ from unity can be explained by $A_U \neq A_T$, $C_{IU} \neq C_{IT}$, or $f_1 \neq g_1$. The first two inequalities are related to differences in the constants of the Rotta model, while the third inequality is caused by dissimilarity in the relaxation time scales. Even if the constants of the Rotta model are taken as the same for momentum and heat fluxes, as in Katul et al. (2014), dissimilarity in the relaxation time scales, as shown in Fig. 3, can still result in a $Pr_{t,\mathrm{neu}}$ differing from unity.

The majority of experiments and simulations suggest that $Pr_{t,\mathrm{neu}} < 1$ but the variability is often significant (Businger et al. 1971; Högström 1996; Venayagamoorthy and Stretch 2006, 2009; Huang et al. 2013). In many turbulence closure schemes used in numerical weather and climate models, $Pr_{t,\mathrm{neu}}$ is often set to unity (Janjić 2002). Using the Weather Research and Forecasting model (Skamarock and Klemp 2008), Tastula et al. (2015) showed that changing the value of $Pr_{t,\mathrm{neu}}$ can affect the moisture profile up to 500 m. Given the significance of $Pr_{t,\mathrm{neu}}$, the generalized cospectral budget model here may provide a framework for understanding the causes of variability of $Pr_{t,\mathrm{neu}}$ and for estimating its value.

4.2 Changes in the Turbulent Energy Spectra with Increasing Stability

Because $\int_0^\infty F_{ww}(k)\mathrm{d}k > 0$ even for $Rf > Rf_{\mathrm{m}}$, Rf_{m} cannot be viewed as a point of incipient laminarization. The analysis in Katul et al. (2014) suggested that Rf_{m} may be viewed as a threshold where the shape of $F_{ww}(k)$ begins to degenerate from its near-neutral and mildly stable form, including a termination of the ISR scaling associated with three-dimensional locally homogeneous and isotropic turbulence. This interpretation of Rf_{m} is consistent with other experimental work (Grachev et al. 2013) that showed, when $Rf > Rf_{\mathrm{m}}$, that ISR scaling no longer holds (but the exact threshold may be Reynolds number dependent). This interpretation is also supported by Fig. 1, where $F_{ww}(k)$ deviates significantly from its idealized shape when $Rf > Rf_{\mathrm{m}}$. At this point, however, it remains unclear why $F_{ww}(k)$ or its integrated form that is connected to the TKE in the vertical direction (denoted as TKE_w) respond to increasing Rf faster than $F_{TT}(k)$ or its integrated form that is connected to the TPE. Recent work demonstrated the significant role of TPE in reproducing the Pr_{t}–Rf relation under stable conditions using the energy- and flux-budget Reynolds-averaged closure model (Zilitinkevich et al. 2007, 2008, 2013). In the energy- and flux-budget model, the impact of increasing Rf on the partition between TKE and TPE was key to re-constructing the Pr_{t}–Rf relation. Can the cospectral budget model here reproduce such energy partition with increasing Rf ? Can the cospectral budget model explain why $F_{ww}(k)$ collapses faster than $F_{TT}(k)$ as Rf approaches Rf_{m}? To address these questions, only the vertical component of TKE (i.e., TKE_w) is considered since it is the component that primarily controls vertical movement opposed or supported by gravity. TKE_w can be derived from the spectra as

$$TKE_w = \frac{1}{2}\int_0^\infty F_{ww}(k)\,\mathrm{d}k = \frac{5}{4}C_o\epsilon^{\frac{2}{3}}k_{a,w}^{-\frac{2}{3}}, \tag{27}$$

and

$$TPE = \frac{1}{2}\frac{\beta^2}{N^2}\int_0^\infty F_{TT}(k)\,\mathrm{d}k = \frac{1}{2}\frac{\beta^2}{N^2}\left[\frac{5}{2} + \ln\left(k_{a,T}\alpha\delta\right)\right]C_T N_T \epsilon^{-\frac{1}{3}}k_{a,T}^{-\frac{2}{3}}. \tag{28}$$

To make progress on the aforementioned list of questions, an assumption of maximum simplicity is to consider the equilibrated TKE and temperature variance budgets in the stable ASL so that $\epsilon = P_m + \beta\overline{w'\theta'} = P_m(1 - R_f)$ and $N_T = -\overline{w'\theta'}\Gamma = 1/\beta\, R_f \Gamma\, P_m$. These estimates can be inserted into the above two equations to yield

$$\frac{TPE}{TKE_w} = Q_2 \frac{C_T}{C_o} \frac{Rf}{1 - Rf}, \tag{29}$$

where

$$Q_2 = \left[1 + \frac{2}{5} \ln\left(k_{a,T}\alpha\delta\right)\right] \left(\frac{k_{a,w}}{k_{a,T}}\right)^{2/3}. \tag{30}$$

Again, to ensure $\epsilon > 0$ (a defining syndrome of turbulent flows), $Rf < 1$. In the range where $0 < Rf < 1$, Eq. 29 shows that TPE/TKE_w increases as Rf increases, which is consistent with the energy- and flux-budget model results (Zilitinkevich et al. 2007, 2008, 2013).

However, the above analysis does not completely answer why the ISR in the spectra of vertical velocity disappears earlier than in the spectra of temperature. To do so, the responses of TKE and TPE to increasing Rf are now further examined in the vicinity of $Rf = Rf_{\mathrm{m}}$. First, the production rate of TKE is derived as a function of Rf. Substituting $\epsilon = P_m + \beta\overline{w'\theta'} = P_m(1 - R_f)$ into Eq. 17 yields

$$\beta\overline{w'\theta'} = -\beta \frac{1 - C_{IT}}{A_T} C_o P_m^{\frac{1}{3}} (1 - R_f)^{\frac{1}{3}} \Gamma g_1 Q, \tag{31}$$

and as a result,

$$-R_f P_m = -\beta \frac{1 - C_{IT}}{A_T} C_o P_m^{\frac{1}{3}} (1 - R_f)^{\frac{1}{3}} \Gamma g_1 Q, \tag{32}$$

$$P_m = \left[\frac{1 - C_{IT}}{A_T} C_o \beta \Gamma g_1 (1 - R_f)^{\frac{1}{3}} Q\right]^{\frac{3}{2}} Rf^{-\frac{3}{2}}. \tag{33}$$

Denoting $w_1 = [1/(1 - C_{IT})](C_T/C_o)(g_2/g_1)$, $w_2 = [(1 - C_{IT})/A_T]C_o\beta\Gamma g_1$, and $w_3 = w_1 + 1$, Eq. 33 can be rearranged to yield

$$P_m = w_2^{\frac{3}{2}} (1 - R_f)^{\frac{1}{2}} \left(1 - w_1 \frac{R_f}{1 - R_f}\right)^{\frac{3}{2}} Rf^{-\frac{3}{2}}. \tag{34}$$

Again, to ensure $P_m > 0$, Rf must satisfy the following: $Rf < 1$ (as earlier noted to maintain finite ϵ) and $Rf < (1/w_3) = Rf_m$. Given that $w_1 \approx 3$ when $g_2 \approx g_1$, $w_3 \approx 4$ and hence $Rf_{\mathrm{m}} \approx 0.25$. The change in P_m with respect to Rf is given by

$$\frac{\mathrm{d}P_m}{\mathrm{d}Rf} = -w_2^{\frac{3}{2}} \frac{(1 - w_3 R_f)^{\frac{1}{2}}}{Rf^{\frac{5}{2}}(Rf - 1)^2} w_3 \left[Rf^2 - \frac{5}{2w_3} Rf + \frac{3}{2w_3}\right]. \tag{35}$$

Provided $w_3 > 25/24$, the quantity $Rf^2 - (5/2w_3)Rf + (3/2w_3) > 0$. This is generally satisfied since $w_3 \approx 4$. Hence, solving $\mathrm{d}P_m/\mathrm{d}Rf = 0$ yields $Rf = 1/w_3 = Rf_m$, and when $Rf < Rf_m$, $\mathrm{d}P_m/\mathrm{d}Rf < 0$. Therefore, when $Rf \to Rf_m$, both P_m and $\mathrm{d}P_m/\mathrm{d}Rf$ become zero, implying that any disturbances near $Rf = Rf_m$ are not likely to alter the state of P_m.

Using similar steps, the production rate of TPE (P_T) is derived and given by

$$P_T = \frac{\beta^2}{N^2} N_T = \frac{\beta^2}{N^2} \frac{1}{\beta} R_f \Gamma\, P_m = RfP_m. \tag{36}$$

Given that P_m is expressed as a function of R_f according to Eq. 34,

$$\frac{\mathrm{d}P_T}{\mathrm{d}Rf} = -w_2^{\frac{3}{2}} \frac{(1 - w_3 R_f)^{\frac{1}{2}}}{Rf^{\frac{3}{2}}(Rf - 1)^2} w_3 \left[\left(1 - \frac{3}{2w_3} \right) Rf + \frac{1}{2w_3} \right]. \tag{37}$$

Noting that for $w_3 \approx 4$, it can be shown that $\mathrm{d}P_T/\mathrm{d}Rf < 0$ in the range of $0 < Rf < Rf_{\mathrm{m}}$ and $\mathrm{d}P_T/\mathrm{d}Rf = 0$ occurs when $Rf = Rf_{\mathrm{m}}$. That is, $Rf = Rf_{\mathrm{m}}$ is also a stable minimum for P_T around which perturbations are difficult to grow.

Given that both production rates of TKE and TPE approach zero when $Rf \to Rf_{\mathrm{m}}$, evaluation of their ratio in the vicinity of Rf_{m} requires evaluation of the ratio of their derivatives with respect to Rf (L'Hôpital's Rule). It can be shown that

$$\frac{\mathrm{d}P_m/\mathrm{d}Rf}{\mathrm{d}P_T/\mathrm{d}Rf} = 1 + \frac{\frac{3}{2w_3}(Rf - 1)^2}{Rf\left[\left(1 - \frac{3}{2w_3} \right) Rf + \frac{1}{2w_3} \right]} > 1. \tag{38}$$

Consequently, no matter what their starting point was when $Rf < Rf_{\mathrm{m}}$, the rate of decay of P_m is faster than P_T with increasing Rf as $Rf \to Rf_{\mathrm{m}}$, which is consistent with observed spectra of vertical velocity collapsing before their temperature counterparts in the vicinity of $Rf = Rf_{\mathrm{m}}$ as shown in Figs. 1 and 2. Interestingly, the earlier collapse of $F_{ww}(k)$ than $F_{TT}(k)$ is in broad agreement with the results from the quasi-normal scale elimination theory, as shown in Galperin and Sukoriansky (2010) and Sukoriansky and Galperin (2013); however, those studies are focused on the transition of '$-5/3$' to '-3' scaling at the Ozmidov wavenumber in both kinetic and potential energy spectra.

In summary, the generalized cospectral budget model reproduces the variation of the partitioning between TKE and TPE with increasing Rf. It also explains why $F_{ww}(k)$ collapses faster than $F_{TT}(k)$ as Rf approaches Rf_{m}.

5 Conclusions

A recently proposed cospectral budget model (Katul et al. 2014) connected a number of features about the stable ASL including the spectral shapes of vertical velocity and temperature, the turbulent Prandtl number, and the existence of a 'maximum flux Richardson number' $Rf_{\mathrm{m}} \approx 0.25$ that was shown not to be tied to laminarization. Critical assumptions leading to those results are examined based on datasets collected over a lake and a glacier, namely, the ideal spectral shapes that follow the '$-5/3$' scaling at high wavenumbers and flatten at low wavenumbers, as well as the similarity between relaxation time scales for momentum and heat fluxes. It is observed that the spectra of temperature follow a '-1' power-law scaling for small wavenumbers and then follow a '$-5/3$' scaling in the ISR for large wavenumbers. The relaxation time scales for momentum and heat fluxes are also found not to be identical. The wavenumbers at which the relaxation time scales undergo transition from the '$-2/3$' power-law scaling to a constant differ for momentum and heat fluxes. The cospectral budget model is then generalized to accommodate these findings and to evaluate their impacts. Results show that the existence of a '-1' scaling law in the spectra of temperature primarily reduces the value of Rf_{m}. The dissimilarity in the relaxation time scales for momentum and heat fluxes in terms of the transition wavenumber primarily alters the turbulent Prandtl number under neutral conditions.

In Katul et al. (2014), Rf_{m} was connected to the maintenance of Kolmogorov scaling in the spectra of vertical velocity and temperature instead of being conventionally interpreted

as the point at which the flow laminarizes. The experiments here support this view and agree with other long-term field experiments (Grachev et al. 2013). However, it was not previously evident why the vertical velocity spectra collapse prior to their temperature counterparts when Rf approaches Rf_{m}. By collapse, we mean that the spectral shapes deviate appreciably from their near-neutral or mildly stable counterparts. It is demonstrated here that the production rate of TKE decreases more rapidly than that of TPE in the vicinity Rf_{m} despite both being quite small. This finding offers a new perspective in explaining why the vertical velocity spectra collapse earlier than their temperature counterparts in the vicinity of Rf_{m}.

More broadly, our results may also explain why dimensional considerations proved to be effective in describing the bulk flow properties for mildly or moderately stable conditions, but failed to do so when $Rf > Rf_{\mathrm{m}}$ (Mahrt 2014). When the energy (kinetic and potential) distribution of eddies experiences a 'transition' to another distribution function, as may occur with the vertical velocity spectra when $Rf > Rf_{\mathrm{m}}$, dimensional considerations and similarity theories may encounter difficulties in predicting the bulk flow properties. Beyond $Rf > Rf_{\mathrm{m}}$, the shapes of spectra (and cospectra) actually change with changing Rf suggesting that a unique eddy-energy distribution does not exist. Because of the links between these energy distributions of eddies and macroscopic or bulk properties of the mean flow, the expected range over which the universal character of stability correction functions or the turbulent Prandtl number exists can be explained.

Acknowledgments DL acknowledges support from the NOAA (U.S. Department of Commerce) Grant NA08OAR4320752 and the Carbon Mitigation Initiative at Princeton University, sponsored by BP. The statements, findings, and conclusions are those of the authors and do not necessarily reflect the views of the NOAA, the U.S. Department of Commerce or BP. GK acknowledges support from the National Science Foundation (NSF-EAR-1344703, NSF-AGS-1102227), the United States Department of Agriculture (2011-67003-30222), the U.S. Department of Energy (DOE) through the office of Biological and Environmental Research (BER) Terrestrial Ecosystem Science (TES) Program (DE-SC0006967 and DE-SC0011461), and the Binational Agricultural Research and Development (BARD) Fund (IS-4374-11C). EBZ acknowledges support from NSF's Physical and Dynamic Meteorology Program under AGS-1026636. The experimental data were collected by the Environmental Fluid Mechanics and Hydrology Laboratory of Professor Marc Parlange at L'École Polytechnique Fédérale de Lausanne.

Appendix: Data and Methodology

The datasets used were collected in the stably stratified ASL over a lake and a glacier surface. These datasets include measurements of three-dimensional velocity and temperature at high frequency (=20 Hz) and at four different heights. Details about the two datasets and quality control measures can be found elsewhere (Vercauteren et al. 2008; Huwald et al. 2009; Bou-Zeid et al. 2010; Li and Bou-Zeid 2011; Li et al. 2012a). In particular, data where fluxes measured at the four heights differ by more than 10 % are excluded. Calculations of turbulent fluxes follow the standard eddy-covariance method with an averaging interval of 30 min (Li and Bou-Zeid 2011; Li et al. 2012a). Calculations of spectra and cospectra for each 30-min segment follow the standard Fourier transform method (Stull 1988), which are then smoothed using a periodic hamming window without overlap. The mean velocity and temperature vertical gradients, which are needed in the calculations of Rf and relaxation time scales, are obtained by fitting second-order polynomial functions to the mean velocity and temperature at the four measurement levels and then taking the derivatives of the fitted functions. A linear interpolation method was also used to compute the vertical gradients of mean velocity and temperature and the results were found to be insensitive to the method of evaluating the vertical gradients, which is consistent with Grachev et al. (2007). The datasets

are separated into eight regimes according to *Rf*, as can be seen from Table 1. Since the lake dataset primarily spans slightly stable to mildly stable conditions and the glacier dataset spans mildly stable to very stable conditions, the first five stability regimes in Table 1 only include data from the lake and the last three regimes only include data from the glacier set. Regime *e* and regime *f* cover roughly the same range of *Rf* but the averaged *Rf* of all segments are different: regime *f* has a much larger averaged *Rf* than regime *e*. The calculated spectra and relaxation time scales for each segment are further averaged over each stability regime, which are shown in Figs. 1, 2, and 3.

References

Ansorge C, Mellado JP (2014) Global intermittency and collapsing turbulence in the stratified planetary boundary layer. Boundary-Layer Meteorol 153(1):89–116

Bos W, Bertoglio J (2007) Inertial range scaling of scalar flux spectra in uniformly sheared turbulence. Phys Fluids 19:025104–025111

Bos W, Touil H, Shao L, Bertogli J (2004) On the behavior of the velocity-scalar cross correlation spectrum in the inertial range. Phys Fluids 16:3818–3823

Bou-Zeid E, Higgins C, Huwald H, Parlange M, Meneveau C (2010) Field study of the dynamics and modelling of subgrid scale turbulence in a stable atmospheric surface layer over a glacier. J Fluid Mech 665:480–515

Bouruet-Aubertot P, Van Haren H, Lelong MP (2010) Stratified inertial subrange inferred from in situ measurements in the bottom boundary layer of the Rockall channel. J Phys Oceanogr 40(11):2401–2417

Businger JA, Yaglom AM (1971) Introduction to Obukhov's paper on 'Turbulence in an atmosphere with a non-uniform temperature'. Boundary-Layer Meteorol 2:3–6

Businger JA, Wyngaard JC, Izumi Y, Bradley EF (1971) Flux–profile relationships in the atmospheric surface layer. J Atmos Sci 28(2):181–191

Calaf M, Hultmark M, Oldroyd H, Simeonov V, Parlange M (2013) Coherent structures and the k^{-1} spectral behaviour. Phys Fluids 25(12):125,107

Cava D, Katul G (2012) On the scaling laws of the velocity-scalar cospectra in the canopy sublayer above tall forests. Boundary-Layer Meteorol 145:351–367

Cava D, Giostra U, Siqueira M, Katul G (2004) Organised motion and radiative perturbations in the nocturnal canopy sublayer above an even-aged pine forest. Boundary-Layer Meteorol 112(1):129–157

Chung D, Matheou G (2012) Direct numerical simulation of stationary homogeneous stratified sheared turbulence. J Fluid Mech 696:434–467

Corrsin S (1961) The reactant concentration spectrum in turbulent mixing with a first-order reaction. J Fluid Mech 11:407–416

Cot C (2001) Equatorial mesoscale wind and temperature fluctuations in the lower atmosphere. J Geophys Res 106(D2):1523–1532

Davidson PA, Kaneda Y, Sreenivasan KR (2012) Ten chapters in turbulence. Cambridge University Press, New York, 450 pp

Derbyshire S (1999) Stable boundary-layer modeling: established approaches and beyond. Boundary-Layer Meteorol 90:423–446

Deusebio E, Brethouwer G, Schlatter P, Lindborg E (2014) A numerical study of the unstratified and stratified Ekman layer. J Fluid Mech 755:672–704

Fernando H (1991) Turbulent mixing in stratified fluids. Annu Rev Fluid Mech 23:455–493

Fernando H, Weil J (2010) Whither the stable boundary layer? A shift in the research agenda. Bull Am Meteorol Soc 91:1475–1484

Foken T (2006) 50 years of the Monin–Obukhov similarity theory. Boundary-Layer Meteorol 19:431–447

Galperin B, Sukoriansky S (2010) Geophysical flows with anisotropic turbulence and dispersive waves: flows with stable stratification. Ocean Dyn 60(5):1319–1337

Galperin B, Sukoriansky S, Anderson PS (2007) On the critical Richardson number in stably stratified turbulence. Atmos Sci Lett 8:65–69

Gioia G, Guttenberg N, Goldenfeld N, Chakraborty P (2010) Spectral theory of the turbulent mean-velocity profile. Phys Rev Lett 105:184501

Grachev A, Andreas E, Fairall C, Guest P, Persson PG (2007) On the turbulent Prandtl number in the stable atmospheric boundary layer. Boundary-Layer Meteorol 125:329–341

Grachev A, Andreas E, Fairall C, Guest P, Persson PG (2013) The critical Richardson number and limits of applicability of local similarity theory in the stable boundary layer. Boundary-Layer Meteorol 147:51–82
Högström U (1996) Review of some basic characteristics of the atmospheric surface layer. In: Boundary-Layer Meteorology 25th Anniversary Volume, 1970–1995, Springer, pp 215–246
Holtslag AAM et al (2013) Stable atmospheric boundary layers and diurnal cycles: challenges for weather and climate models. Bull Am Meteorol Soc 94:1691–1706
Howard LN (1961) Note on a paper of John W. Miles. J Fluid Mech 10(4):509–512
Huang J, Bou-Zeid E, Golaz JC (2013) Turbulence and vertical fluxes in the stable atmospheric boundary layer. Part 2: A novel mixing-length model. J Atmos Sci 70(6):1528–1542
Huwald H, Higgins C, Boldi M, Bou-Zeid E, Lehning M, Parlange M (2009) Albedo effect on radiative errors in air temperature measurements. Water Resour Res 45:W08431
Ishihara T, Yoshida K, Kaneda Y (2002) Anisotropic velocity correlation spectrum at small scales in a homogeneous turbulent shear flow. Phys Rev Lett 88:154501
Janjić ZI (2002) Nonsingular implementation of the Mellor–Yamada level 2.5 scheme in the ncep meso model. NCEP office note 437:61
Kader B, Yaglom A (1991) Spectra and correlation functions of surface layer atmospheric turbulence in unstable thermal stratification. In: Metais O, Lesieur M (eds) Turbulence and coherent structures. Kluwer Academic Publishers, Boston, pp 450–467
Kaimal J, Finnigan J (1994) Atmospheric boundary layer flows: their structure and measurement. Oxford University Press, New York, 289 pp
Kaimal JC (1973) Turbulence spectra, length scales and structure parameters in the stable surface layer. Boundary-Layer Meteorol 4:289–309
Kaimal JC, Izumi Y, Wyngaard JC, Cote R (1972) Spectral characteristics of surface-layer turbulence. Q J R Meterol Soc 98(417):563–589
Katul G, Chu C (1998) A theoretical and experimental investigation of energy-containing scales in the dynamic sublayer of boundary-layer flows. Boundary-Layer Meteorol 86:279–312
Katul G, Manes C (2014) Cospectral budget of turbulence explains the bulk properties of smooth pipe flow. Phys Rev E 90(063):008
Katul G, Chu C, Parlange M, Albertson J, Ortenburger T (1995) Low-wavenumber spectral characteristics of velocity and temperature in the atmospheric surface layer. J Geophys Res 100(D7):14,243–14,255
Katul G, Albertson J, Hsieh C, Conklin P, Sigmon J, Parlange M, Knoerr K (1996) The 'inactive' eddy motion and the large-scale turbulent pressure fluctuations in the dynamic sublayer. J Atmos Sci 53(17):2512–2524
Katul G, Schieldge J, Hsieh CI, Vidakovic B (1998) Skin temperature perturbations induced by surface layer turbulence above a grass surface. Water Resour Res 34(5):1265–1274
Katul G, Mahrt L, Poggi D, Sanz C (2004) One and two equation models for canopy turbulence. Boundary-Layer Meteorol 113:81–109
Katul G, Konings A, Porporato A (2011) Mean velocity profile in a sheared and thermally stratified atmospheric boundary layer. Phys Rev Lett 107:268502
Katul G, Porporato A, Nikora V (2012) Existence of k^{-1} power-law scaling in the equilibrium regions of wall-bounded turbulence explained by Heisenberg's eddy viscosity. Phys Rev E 86(1):066311
Katul G, Li D, Chamecki M, Bou-Zeid E (2013) Mean scalar concentration profile in a sheared and thermally stratified atmospheric surface layer. Phys Rev E 87(2):023004
Katul G, Porporato A, Shah S, Bou-Zeid E (2014) Two phenomenological constants explain similarity laws in stably stratified turbulence. Phys Rev E 89(1):023007
Kays W (1994) Turbulent Prandtl number—where are we? J Heat Transf 116:284–295
Kolmogorov A (1941a) Dissipation of energy under locally isotropic turbulence. Dokl Akad Naukl SSSR 32:16–18
Kolmogorov A (1941b) The local structure of turbulence in imcompressible viscous fluid for very large Reynolds numbers. Dokl Akad Naukl SSSR 30:299–303
Launder B, Reece G, Rodi W (1975) Progress in the development of a Reynolds-stress turbulence closure. J Fluid Mech 68:537–566
Li D, Bou-Zeid E (2011) Coherent structures and the dissimilarity of turbulent transport of momentum and scalars in the unstable atmospheric surface layer. Boundary-Layer Meteorol 140(2):243–262
Li D, Bou-Zeid E, de Bruin H (2012a) Monin–Obukhov similarity functions for the structure parameters of temperature and humidity. Boundary-Layer Meteorol 145(1):45–67
Li D, Katul G, Bou-Zeid E (2012b) Mean velocity and temperature profiles in a sheared diabatic turbulent boundary layer. Phys Fluids 24(10):105105
Li D, Katul G, Zilitinkevich S (2015) Revisiting the turbulent Prandtl number in an idealized atmospheric surface layer. J Atmos Sci 72(6):2394–2410

Lumley J (1967) Similarity and the turbulent energy spectrum. Phys Fluids 10:855–858
Mahrt L (1999) Stratified atmospheric boundary layers. Boundary-Layer Meteorol 90:375–396
Mahrt L (2014) Stably stratified atmospheric boundary layers. Annu Rev Fluid Mech 46:23–45
Miles J, Howard L (1964) Note on heterogeneous shear flow. J Fluid Mech 20:331–336
Miles JW (1961) On the stability of heterogeneous shear flows. J Fluid Mech 10(04):496–508
Monin A, Obukhov A (1954) Basic laws of turbulent mixing in the ground layer of the atmosphere. Akad Nauk SSSR Geofiz Inst Trudy 151:163–187
Monin A, Yaglom A (1971) Statistical fluid mechanics, vol 1. MIT Press, Cambridge, 782 pp
Obukhov A (1946) Turbulence in thermally inhomogeneous atmosphere. Trudy Inta Teoret Geofiz Akad Nauk SSSR, pp 95–115
Perry A, Henbest S, Chong M (1986) A theoretical and experimental study of wall turbulence. J Fluid Mech 165:163–199
Perry AE, Abell CJ (1975) Scaling laws for pipe-flow turbulence. J Fluid Mech 67:257–271
Perry AE, Abell CJ (1977) Asymptotic similarity of turbulence structures in smooth- and rough-walled pipes. J Fluid Mech 79:785–799
Pond S, Smith S, Hamblin P, Burling R (1966) Spectra of velocity and temperature fluctuations in the atmospheric boundary layer over the sea. J Atmos Sci 23:376–386
Pope S (2000) Turbulent flows. Cambridge University Press, Cambridge, 802 pp
Poulos GS, Blumen W, Fritts DC, Lundquist JK, Sun J, Burns SP, Nappo C, Banta R, Newsom R, Cuxart J et al (2002) CASES-99: a comprehensive investigation of the stable nocturnal boundary layer. Bull Am Meteorol Soc 83(4):555–558
Riley JJ, Lindborg E (2008) Stratified turbulence: a possible interpretation of some geophysical turbulence measurements. J Atmos Sci 65(7):2416–2424
Salesky S, Katul G, Chamecki M (2013) Buoyancy effects on the integral length scales and mean velocity profile in atmospheric surface layer flows. Phys Fluids 25(10):105101
Sandu I, Beljaars A, Bechtold P, Mauritsen T, Balsamo G (2013) Why is it so difficult to represent stably stratified conditions in numerical weather prediction (NWP) models? J Adv Model Earth Syst 5:117–133
Skamarock WC, Klemp JB (2008) A time-split nonhydrostatic atmospheric model for weather research and forecasting applications. J Comput Phys 227(7):3465–3485
Sorbjan Z (2006) Local structure of turbulence in stably stratified boundary layers. J Atmos Sci 63(5):1526–1537
Sorbjan Z (2010) Gradient-based scales and similarity laws in the stable boundary layer. Q J R Meterol Soc 136(650):1243–1254
Stull R (1988) An introduction to boundary layer meteorology. Kluwer Academic Publishers, Dordrecht, 670 pp
Sukoriansky S, Galperin B (2013) An analytical theory of the buoyancy-Kolmogorov subrange transition in turbulent flows with stable stratification. Philos Trans R Soc A 371(1982):0120,212
Sukoriansky S, Galperin B, Perov V (2005a) Application of a new spectral theory of stably stratified turbulence to the atmospheric boundary layer over sea ice. Boundary-Layer Meteorol 117(2):231–257
Sukoriansky S, Galperin B, Staroselsky I (2005b) A quasinormal scale elimination model of turbulent flows with stable stratification. Phys Fluids 17(8):085,107
Sukoriansky S, Galperin B, Perov V (2006) A quasi-normal scale elimination model of turbulence and its application to stably stratified flows. Nonlinear Process Geophys 13(1):9–22
Tastula EM, Galperin B, Dudhia J, LeMone MA, Sukoriansky S, Vihma T (2015) Methodical assessment of the differences between the QNSE and MYJ PBL schemes for stable conditions. Q J R Meterol Soc. doi:10.1002/qj.2503
Taylor G (1938) The spectrum of turbulence. Proc R Soc A 132:476–490
Townsend A (1976) The structure of turbulent shear flow. Cambridge University Press, UK, 442 pp
Venayagamoorthy S, Stretch D (2009) On the turbulent Prandtl number in homogeneous stably stratified turbulence. J Fluid Mech 644:359–369
Venayagamoorthy SK, Stretch DD (2006) Lagrangian mixing in decaying stably stratified turbulence. J Fluid Mech 564:197–226
Vercauteren N, Bou-Zeid E, Parlange MB, Lemmin U, Huwald H, Selker J, Meneveau C (2008) Subgrid-scale dynamics for water vapor, heat, and momentum over a lake. Boundary-Layer Meteorol 128(2):205–228
Wyngaard J, Cote O (1972) Co-spectral similarity theory in the atmospheric surface layer. Q J R Meterol Soc 98:590–603
Yamada T (1975) The critical Richardson number and the ratio of the eddy transport coefficients obtained from a turbulence closure model. J Atmos Sci 32:926–933

Zhang Y, Gao Z, Li D, Li Y, Zhang N, Zhao X, Chen J (2014) On the computation of planetary boundary-layer height using the bulk Richardson number method. Geosci Model Dev 7(6):2599–2611

Zilitinkevich S, Elperin T, Kleeorin N, Rogachevskii I (2007) Energy- and flux-budget (EFB) turbulence closure model for stably stratified flows. Part I: Steady-state, homogeneous regimes. Boundary-Layer Meteorol 125:167–192

Zilitinkevich S, Elperin T, Kleeorin N, Rogachevskii I, Esau I, Mauritsen T, Miles M (2008) Turbulence energetics in stably stratified geophysical flows: strong and weak mixing regimes. Q J R Meteorol Soc 134:793–799

Zilitinkevich S, Elperin T, Kleeorin N, Rogachevskii I, Esau I (2013) A hierarchy of energy- and flux-budget (EFB) turbulence closure models for stably-stratified geophysical flows. Boundary-Layer Meteorol 146:341–373